Design and Analysis of an Integrated Modular Motor Drive for More Electric Aircraft

Shaopeng Wu, *Senior Member, IEEE,* Chenchen Tian, Weiduo Zhao and Jinyang Zhou

***Abstract*— Though many permanent magnet synchronous motors (PMSM) are used as the driving source for aerospace applications, the motor and converter are not integrated. This leads to large volume and low power density of the system. This paper proposes a SiC-based Integrated Modular Motor Drive (IMMD) as a potential solution, in which the SiC converter is placed at the end of the stator core of the motor. The converter is directly connected to the end-turn windings of the motor so as to reduce wiring cable losses, with the motor and converter being cooled by an integrated water-cooled housing, significantly reducing the weight of the system and improving the power density. First, the topology of a five-phase IMMD is briefly introduced. Then, the influence of the number of slots on the output performance of the motor is analyzed with the aim of improving the power density of the system. Because the system integration will cause the loss density of the motor to increase sharply, this will thereby cause the local temperature of the IMMD to be higher. A detailed analysis and calculation of the thermal design will be required to improve the reliability of the system in high temperature environments. The skewed rotor method is adopted so that the torque ripple of the fractional-slot motor is suppressed in the high-speed region. The results show that these methods can increase the power density of the IMMD and expand the speed range of the motor so as to meet the needs of different stages during the whole flight of more electric aircraft.**

***Index Terms*—Integrated, modular motor drives, permanent magnet synchronous motor, more electric aircraft.**

I. INTRODUCTION

A SHIFT from motors and driving systems that were traditionally physically separated to more compact, high power density motor-drive combinations has occurred over the last two decades [1]. In recent years, electric driving systems have gradually replaced traditional hydraulic or pneumatic systems in the driving of more electric aircrafts. Compared with traditional power systems, aerospace motor driving systems have the advantage of being lightweight, highly efficient and small in size, which can greatly improve dynamic performance. Though traditional aircraft power systems use a hydraulic or pneumatic system with high reliability, this leads to a complex system structure, low efficiency, high maintenance costs and a high cycle time, with it being increasingly difficult to meet the requirements of modern high-performance more electric aircrafts [2].

As the aerospace field has high requirements concerning power density, reliability and the conversion efficiency of the driving system, in the early days, due to the low level of technology, three-phase asynchronous motors and DC brushed motors were mostly used as aerospace motors. With continuous improvements in the performance of permanent magnet materials, some new types of motors have become widely used in the field of aviation, such as DC brushless motors [3], permanent magnet synchronous motors (PMSM) [4], and switched reluctance motors. These new motors have many advantages, including higher conversion efficiency and a wider operating speed range.

In a conventional motor driving system, the motor and converter are often placed in separate cabinets, reducing manufacturing costs and difficulties, but also leading to the driving system being of a larger weight and volume, thereby greatly decreasing the power density of the whole system. Long wire cables between the motor and the converter cause excessive losses and electromagnetic interference, further causing large torque ripples in the driving system and affecting the normal operation of the system. One potential solution to all of this is Integrated Motor Drives (IMD). It is beneficial to the overall reduction of invalid losses to integrate the motor and converter together, installing it on the integrally formed housing and connecting the motor windings and the converter directly through short wire cables. It is possible to use a unified cooling housing for the motor and converter, greatly reducing the mass and volume of the motor and the converter and thereby greatly improving the power density of the driving system. However, the motor and converter cannot be simply combined at the physical level; the converter will be affected by the complex electromagnetic field environment of the motor, with difficulty in controls and system instability increasing and the output of the entire performance of the driving system therefore being affected.

An IMD developed by the University of Wisconsin-Madison has high power density, torque density and fault tolerance. The stator core is made of a soft magnetic composite. This method can provide greater flexibility, more phases, as well as separated teeth and coils. Furthermore, it is convenient for modular forming and the placement of concentrated windings. These teeth and coils can be directly connected to the

Manuscript received January 31, 2020; revised February 26 2020; accepted May 1 2020. This work was supported in part by the Power Electronics Science and Education Development Program of Delta Group (DREM2019004), and in part by the National Natural Science Foundation of China under Grant 51977049 and the Heilongjiang Province Natural Science Foundation of China under Grant E2018034.

S. Wu, C. Tian, J. Zhou are with the Department of Electrical Engineering, Harbin Institute of Technology, Harbin 150080, China (e-mail: wushaopeng@hit.edu.cn, 13115303230@163.com, s96123@163.com).

Weiduo Zhao is with Key Laboratory of More Electric Aircraft Technology of Zhejiang Province, University of Nottingham Ningbo China. (e-mail: zhaoweiduo@gmail.com).

This article has been accepted for publication in a future issue of this journal, but has not been fully edited. Content may change prior to final publication. Citation information: DOI 10.1109/TTE.2020.2992901, IEEE Transactions on Transportation Electrification

control side port so that the control part is more closely combined with the stator teeth, forming the real component of the integrated system [5]. A distributed converter integrates a ring converter at the end of the motor [6]. The distributed power electronics reduce the system volume and have a higher degree of freedom in the control of the motor.

Research on the application of five-phase fault tolerant motors in aircraft has been published [7]. Through the study of multiphase motors with different phases and slots, Hennen derives the harmonic formulas of different motors, with multiple prototypes of multiphase motors being designed [8], [9]. The results show that, when compared to a three-phase motor of the same power, the mass of a multiphase motor can be reduced by 30%, with it being possible to reduce the torque ripple by 40%. The harmonic components of fractional-slot windings were analyzed and the eddy current losses of the magnetic steel with harmonic components were quantified, proposing a general method for selecting the optimal slot pole number for the fractional-slot windings [10]. In some literatures, only natural cooling method are applied for the SiC cooling for IMD. The PMSM in this paper has high power rating. The temperature of motor is high and has much more potential risk for the normal operation of SiC components keeping nominal performance. The unified water cooling topology is presented to increase the power density by integrated the cooling method of SiC base plate and casing cooling of motor. The unified cooling method can increase the cooling efficiency and reduce the volume of cooling system. The SiC base plate with annular cooling channels can also be as the shield of electromagnetic field to protect the controller from EMC. The U-shaped PM rotor with two magnetic bridge is presented in the PMSM in which the torque ripple in the high speed point is much decreased. The torque ripple is very important for the reliability, life and comport for passengers and pilots.

In section II, a five-phase IMMD for more electric aircraft applications is proposed. By combining the motor and converter inside a unified housing, the end-turn windings and the converter are directly connected together. This greatly increases the power density of the driving system. The motor and converter cannot be simply combined at the physical level. In order to achieve the requirements of high power density, that is, high-speed range and a high thermal management capability for the IMMD, the number of pole-slot selections and winding matching methods of the IMMD are required. Control strategy and cooling designs for detailed analysis and comparison are slightly different from traditional separate motor and converter designs. In this paper, a five-phase fractional-slot distributed winding permanent magnet synchronous motor is used as an example in order to analyze and explain the design principles of IMMD. The physical topology of the five-phase IMMD is established, with the problems needing attention during the research then being analyzed. In section III, the methods for improving the power density of the IMMD are introduced. On the basis of the motor, the IMMD structure and cooling housing are improved and optimized so as to discover the distribution law. In section IV, analysis is given of the method for eliminating the large torque ripple of the motor at the high speed region due to fractional-slot winding. Further analysis is given of what influences the different skew angles of magnetic poles and segment numbers of the rotor have on the output torque ripple, efficiency and output performance. Based on this, the advantages and disadvantages of the IMMD and the fields of use are analyzed.

II. Integrated Motor Topology

Aircraft in the field of aerospace has very strict requirements regarding the weight of the driving system. The smaller the volume and weight of the driving system, the more items that can be carried. Therefore, the integrated structure design of the motor and the converter can successfully reduce the size and weight, achieving the requirements of system miniaturization. In the entire driving system, the motor, as an electromechanical energy conversion unit, is the core component of the entire system. The performance of the motor will directly affect the operation of the entire more electric aircraft.

A. System Performance Requirements of Motor

The main specifications of the motor developed in this paper are shown in Table I. In the field of aerospace, the performance requirements for motors are highly demanding. Compared with traditional separate motor drives, the mass and volume of the motor system are greatly reduced, leading to a higher loss density per volume of the integrated motor drives. The heat dissipation area decreases sharply, which is not conducive to the heat dissipation of either the motor or the converter. As a driving motor, the aerospace motor has a wide range of speed and a high maximum speed, positing higher requirements for the design of the motor.

TABLE I
Main Specifications of IMMD Motor

Parameters	Value
peak power	110 kW
peak speed	15, 000 rpm
base speed	6000 rpm
maximum efficiency	>96%
power density	1.7 kW/kg

In summary, the design of aerospace motors needs to consider multiple factors, including electromagnetic, mechanical and thermal aspects, in order to meet the requirements of the design indicators.

B. Motor Topology

According to the application environment of aerospace motors, it is necessary to analyze and select various structural parameters and forms of permanent magnet synchronous motors so as to summarize the suitable design guidelines and precautions for IMMD.

TABLE II
Characteristic Dimensions of the Model Considered for FEA Simulations

Parameters	Value
stator outer diameter	260 mm
stator inner diameter	158 mm
axial length	90 mm
air gap length	1 mm
number of pole slots	8/20
pitch	2
magnetic poles distribution type	U

Maxwell software is used for multiple simulations, with the stator and rotor structure parameters of the motor being

This article has been accepted for publication in a future issue of this journal, but has not been fully edited. Content may change prior to final publication. Citation information: DOI 10.1109/TTE.2020.2992901, IEEE Transactions on Transportation Electrification

continuously optimized so that the output performance of the motor is gradually close to optimal. The main characteristic dimensions of the integrated motor can be seen in Table II.

As can be seen from the two-dimensional figure of the motor shown in Fig. 1, the motor of IMMD uses fractional-slot distributed winding, a twenty-slot-eight-pole stator structure and a "U" distribution type magnetic pole structure, resulting in lower mutual inductance, a higher winding coefficient, a higher salient pole ratio and fewer magnetic poles. For multiphase motors, fractional-slot windings are often used, which are relatively simple to manufacture. Its high torque density, low torque ripple and fault tolerance are common in integrated motor drives. The five-phase windings are inserted into twenty stator slots. The five-phase motor can still operate for a short time if a short circuit or open circuit fault occurs in one phase, thereby improving the reliability of the motor.

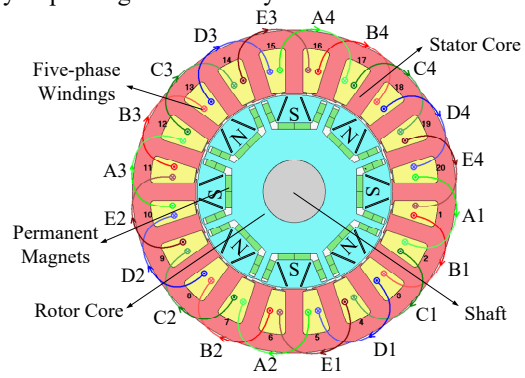

Fig. 1. Schematic diagram of the two-dimensional model of the motor.

As can be seen from the magnetic density cloud of the motor shown in Fig. 2, the magnetic flux density distribution of the motor is reasonable. The highest magnetic density is located at the magnetic bridge of the motor, which is 2.65 T. The magnetic bridge is in a saturated state and has a large magnetic resistance. The magnetic density of the motor tooth is 1.4 T. The magnetic density of the yoke of the motor is 0.6 T, which is not in a saturated state and thus meets the requirements of silicon steel sheet work.

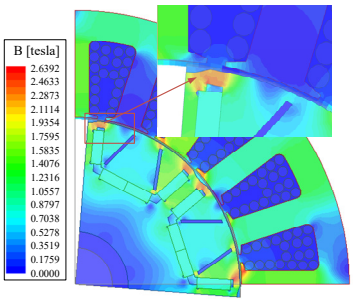

Fig. 2. Magnetic density cloud of the motor.

C. Driver Layout

The overall layout of IMMD and vector control system of the five-phase IMMD during a normal operation is shown in Fig. 3. Five-phase motors have greater torque output and fault tolerance compared to traditional three-phase permanent magnet synchronous motors and are designed based on the NTV-SVPWM (Near Two Vectors SVPWM) algorithm for fault-tolerant algorithms. A comparison and analysis is given of the electromagnetic characteristics before and after applying the fault-tolerant control strategy. The five-phase motor control system based on the NTV-SVPWM algorithm is shown in Fig. 3. For the interior permanent magnet synchronous motor, the stability of the electromagnetic torque is directly related to the quadrature axis current. When the motor is running normally, the MTPA vector control strategy is used to control the electromagnetic torque by adjusting the fundamental wave component in the quadrature axis current after decoupling.

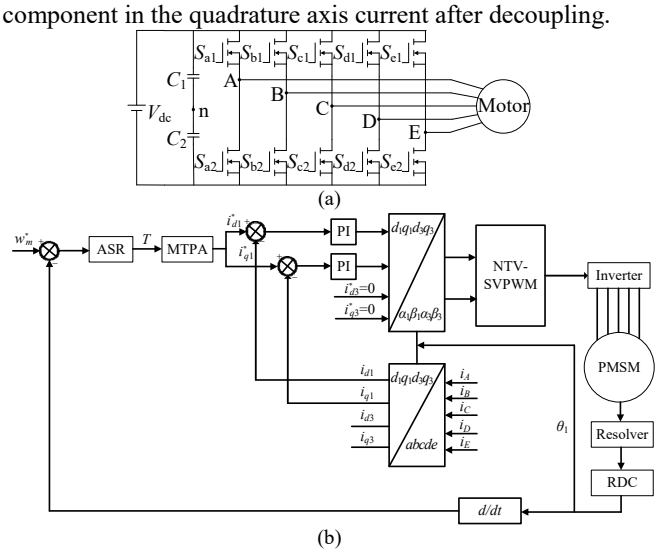

Fig. 3. The schematic diagram of five-phase IMMD control under normal operation. (a) System layout. (b) Schematic diagram of double closed-loop space vector control.

In Simulink, the NTV-SVPWM and NFV-SVPWM (Near Four Vectors SVPWM) simulation algorithm is built, with the control algorithm being verified using an ideal permanent magnet synchronous motor. Taking the phase A current as an example, the ideal current waveform is a standard sine wave. The output current waveform is greatly distorted after filtering the modulated waveform. After Fourier decomposition of the current waveform, it is found that the driving current contains a high third-harmonic component. Using this SVPWM algorithm to drive a five-phase motor, the amplitude and phase of the third harmonic current needs to be handled reasonably so that the harmonic magnetomotive force generated by the third harmonic current can be compared with the third harmonic current in the motor body. Harmonic magnetic fields interact to generate the third harmonic torque, thereby improving the torque output capability of the motor. Fig. 4 shows the current wave of NTV-SVPWM and NFV-SVPWM.

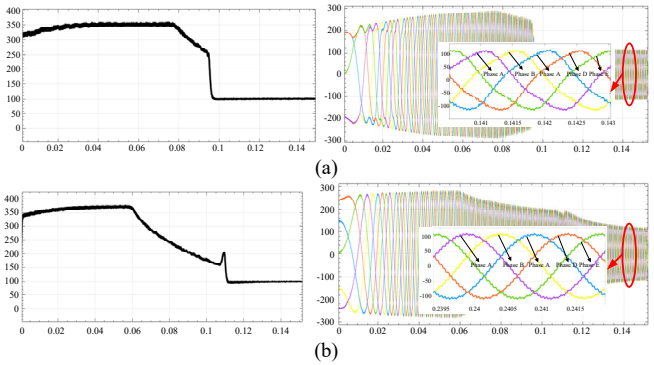

Fig. 4. The current and torque waveforms obtained by two SVPWM algorithms. (a) The torque and current wave of NTV-SVPWM. (b) The torque and current wave of NFV-SVPWM.

When a traditional three-phase motor fails, the motor will not

This article has been accepted for publication in a future issue of this journal, but has not been fully edited. Content may change prior to final publication. Citation information: DOI 10.1109/TTE.2020.2992901, IEEE Transactions on Transportation Electrification

run normally if there is no centerline lead. A five-phase motor can still form a circular rotation when the current of the remaining phases is changed due to an increase in the number of phases. Magnetic fields ensure that the motor can continue to run. Assume that phase A is broken and the current of phase A becomes 0. The amplitude and phase of the remaining four-phase currents need to be changed so as to ensure that the circular rotating magnetic field of the motor does not change. The relationship between the amplitude and phase of the residual phase current is shown in (1).

$$\begin{aligned}\frac{5}{2}I_m\cos(\omega t+\psi)&=(I'_B+I'_E)\cos(\omega t+\frac{2\pi}{5}+\psi)+(I'_c+I'_d)\cos(\omega t+\frac{4\pi}{5}+\psi)\\ \frac{5}{2}I_m\sin(\omega t+\psi)&=(I'_B-I'_E)\sin(\omega t+\frac{2\pi}{5}+\psi)+(I'_c-I'_d)\sin(\omega t+\frac{4\pi}{5}+\psi)\end{aligned} \quad (1)$$

The motor uses a Y-type connection, with the combined vector of the other phase currents being zero. After phase A is open, the specific amplitudes and phases of the remaining phase currents can be obtained through theoretical analysis, as shown in (2), ψ is inner power factor angle.

$$\begin{aligned}I'_B&=1.382I_m\cos(\theta-\frac{\pi}{5}+\psi)\\ I'_C&=1.382I_m\cos(\theta-\frac{4\pi}{5}+\psi)\\ I'_D&=1.382I_m\cos(\theta+\frac{4\pi}{5}+\psi)\\ I'_E&=1.382I_m\cos(\theta+\frac{\pi}{5}+\psi)\end{aligned} \quad (2)$$

The motor adopts constant current amplitude hysteresis control when the phase A is open, with the simulation results of this being shown in Fig. 5. It can be found from Fig. 5 that when the phase A of the motor is disconnected, the output torque of the motor is greatly reduced, and the torque ripple is also greatly increased; when the remaining four-phase winding uses the same amplitude current as the control target for fault tolerance control, the output torque under fault-tolerant control is not much different from the output torque during normal operation, and the torque ripple is large, but compared to the motor without fault-tolerant control, the torque ripple has been greatly reduced.

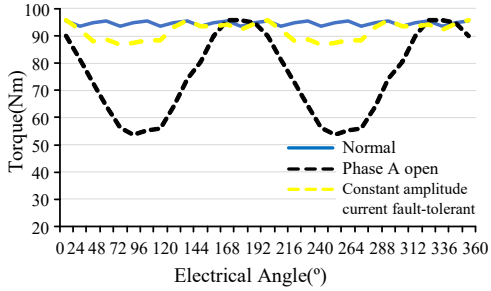

Fig. 5. The output torque of normal, phase A open and constant amplitude current fault-tolerant conditions.

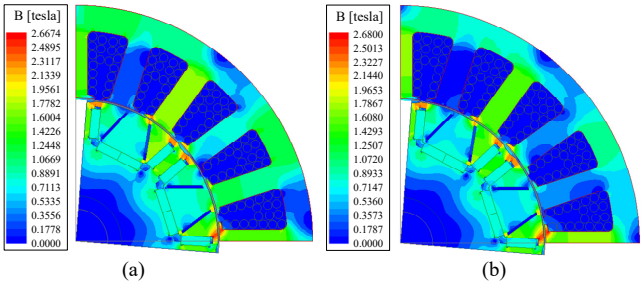

Fig. 6. The cloud map of the magnetic density distribution. (a) Open circuit of phase A. (b) Constant amplitude current fault control.

Fig. 6 shows the cloud map of the magnetic density distribution when the motor is working normally and during constant amplitude current fault-tolerant.

D. IMMD Structure

The converter is placed in the stator iron core end in order to meet the high power density and high-efficiency design indicators of an IMMD system. This structure can reduce the length and losses of the wiring cables of the motor and the converter. The converter and the motor share a water-cooled housing, thereby greatly reducing the volume and weight and improving the power density of IMMD. Compared with the traditional separate motor and converter, in placing the converter of the integrated motor driver behind the iron core end of the motor stator, the temperature distribution of the motor converter will be affected by the motor temperature field. This is due to the motor converter losses, which mainly come from the switching losses of the transmission cables, where only the devices SiC and GaN are used in the integrated motor converter. The high-frequency switching losses of the power device are relatively high compared to the core losses and copper loss of the motor side. The temperature distribution of the converter will be greatly affected by the heat on the motor side as a result of the converter being close to the high temperature structure of the motor end-turn winding and the stator core. The three-dimensional structure of the IMMD is shown in Fig. 7.

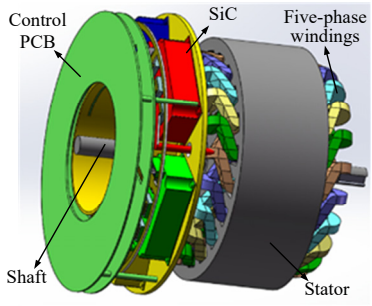

Fig. 7. Three-dimensional structure of the SiC-based five-phase IMMD (without casing and endplates).

III. Methods for Increasing Power Density

Below, analysis is given of three methods with the aim of further improving the power density of IMMD and further reducing its volume and weight.

A. Motor Pole Slot Matching

The selection of the pole-to-slot ratio of the permanent magnet synchronous motor has a major impact on motor performance. According to the basic theory of winding, the expression of the number of slots per pole per phase q is:

$$q=\frac{Q}{2pm} \quad (3)$$

where Q is the total number of motor slots, p is the number of pole pairs, and m is the number of phases. For conventional multiphase motors, the use of fractional-slot concentrated windings is beneficial in greatly reducing the copper losses at the end-turn of the motor at higher winding coefficients. Slot distributed winding reduces difficulty in the manufacturing process. Moreover, it also reduces the influence of the

This article has been accepted for publication in a future issue of this journal, but has not been fully edited. Content may change prior to final publication. Citation information: DOI 10.1109/TTE.2020.2992901, IEEE Transactions on Transportation Electrification

sinusoidal degree of the air gap flux density of the motor due to the slotting of the stator such that the cogging torque of the motor and the torque ripple are small. There are no fractional harmonics in the winding magnetomotive force of the integral-slot motor, the harmonic component of the spatial magnetomotive force is low, and the rotor losses are low. For integral-slot and fractional-slot motors, consideration needs to be given to the sinusoidal degree of the back-EMF of the motor, the eddy current losses of the rotor magnet steel, the cogging torque, as well as other motor performances. According to the design requirements of high power density motors for more electric aircraft, two design schemes are selected for the pole slots of the motors: those of ten-slot-eight-pole and twenty-slot-eight-pole. The former uses fractional-slot concentrated winding, with the latter using fractional-slot distributed windings while keeping the outer diameter of the stator of the motor and the structure of the rotor unchanged. The simulation analysis of two schemes with different pole slots can obtain the no-load back-EMF waveforms of the two schemes under one electrical cycle.

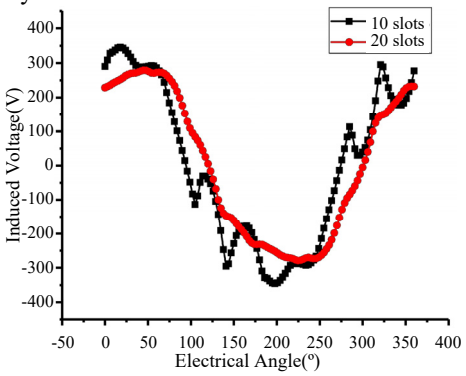

Fig. 8. Back-EMF waveforms of motors with different slots.

As can be seen from the back-EMF waveforms in Fig. 8, it can be concluded that the motor has a poor back-EMF waveform, that the number of the slots is ten, the harmonic content is very rich, and the electric potential peak is high. Furthermore, the motor has a good back-EMF waveform, the number of the slots is twenty, and the harmonics content is small. Through simulation analysis, the peak-to-peak cogging torque of the motor is 0.37 Nm for the ten-slot case and 1.24 Nm for the twenty-slot case under no-load conditions. By simulating the load at a base speed of 6000 rpm, it is found that when the number of poles is constant, the fractional harmonics of the fractional-slot motor will produce large eddy current losses in the permanent magnet. The permanent magnet eddy current losses of the ten-slot and twenty-slot motors are 323.6 W and 23.4W, respectively. The eddy current losses of the two structures are somewhat different. This loss will be more apparent under a high-speed range, which indirectly affects the reliability of aerospace machines. The twenty-slot topology is therefore used in order to reduce the temperature rise of the motor in the high speed area.

Fig. 9 shows a torque and inner power factor angle characteristic diagram for the above two winding structures. At any current angle, the reluctance torque of a twenty-slot-eight-pole motor is greater than a ten-slot-eight-pole fractional-slot concentrated winding motor. At the maximum torque current angle, the reluctance torque of the twenty-slot-eight-pole motor accounts for 37.3%, with the reluctance torque of the ten-slot-eight-pole motor accounting for 23.4%. The armature response magnetic field lines of the two winding structures were analyzed in order to clarify the cause of this occurrence. For a ten-slot-eight-pole motor, the distribution of magnetic field lines under each permanent magnet pole is different, whereas for a twenty-slot-eight-pole motor, the distribution of magnetic field lines under each permanent magnet pole is the same. This phenomenon of a slot concentrated winding permanent magnet motor is denoted as unbalanced armature response. As a result of this unbalanced armature response, some permanent magnets cannot contribute to the reluctance torque during the operation of the motor, ultimately reducing the torque. Therefore, in order to increase the reluctance torque of a fractional-slot winding PMSM, the unbalanced armature response of the motor should be reduced as much as possible, achievable through the optimization of the slot ratio of the motor and the design of the rotor structure.

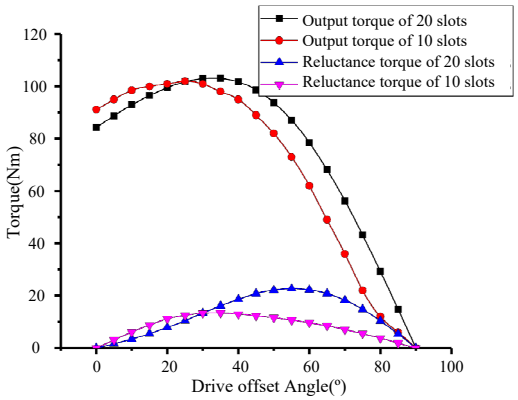

Fig. 9. Torque and inner power factor angle characteristic diagram with different winding structures.

B. *Cooling Optimization*

The distribution of temperature is one of the main factors that affects the performance of the motor. When the temperature of the motor exceeds the insulation level, the insulating material will be damaged. Furthermore, the permanent magnet will be irreversibly demagnetized, seriously shortening the service life of the motor. At present, temperature rise calculation methods mainly consist of three different types: the finite element method, equivalent thermal network method and simplified formula method. The heat of the motor is mainly generated by the copper and iron loss inside the motor, with the heat dissipation being composed of convection heat dissipation, radiation heat dissipation and heat conduction. A small proportion of the motor's energy conduction process is accounted for by radiation heat dissipation. In this paper, the equivalent thermal network method is used, with the motor losses that are introduced into the thermal circuit model for thermal analysis used as the heat source.

There are similarities between the calculation method followed by the thermal network method and the circuit calculation principle. The basic laws of the circuit, such as Kirchhoff's law, will be applicable to the thermal network method. The core aim of thermal network construction is to clarify the internal heat transfer method of the motor and accurately estimate the thermal resistance and heat flow. The formulas for calculating the thermal resistance of heat

This article has been accepted for publication in a future issue of this journal, but has not been fully edited. Content may change prior to final publication. Citation information: DOI 10.1109/TTE.2020.2992901, IEEE Transactions on Transportation Electrification

conduction and convection in a motor are:

$$R_{cd} = \frac{t}{\lambda A} \tag{4}$$

$$R_{dl} = \frac{1}{hA} \tag{5}$$

where t is the heat transfer distance, λ is the thermal conductivity, A is the area of the isothermal surface (that is, the area perpendicular to the direction of the heat flow), and h is the heat dissipation coefficient.

The equivalent thermal resistance can be obtained by bringing into (4) and (5) the obtained equivalent core, the permanent magnet, winding and air-gap thermal conductivity.

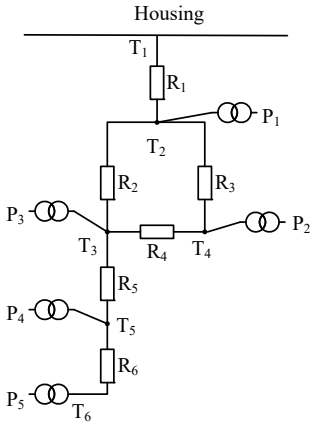

Fig. 10. Simplified thermal network model of motor.

Using the motor in this paper as an example, a particular cogging width of the motor is selected to build a thermal network model, as shown in Fig. 10. Being that wind friction loss is the heat generated by the friction between the rotor surface and air, it is added to the rotor surface as a heat source. The symbols used in Fig. 10 stand for the following: T_1 is the case temperature node; T_2 is the stator yoke temperature node; T_3 is the stator winding temperature node; T_4 is the stator tooth temperature node; T_5 is the rotor surface and air gap temperature node; T_6 is the permanent magnet temperature node; R_1 is the thermal resistance between the casing and the stator yoke; R_2 is the thermal resistance between the stator yoke and the winding; R_3 is the thermal resistance between the stator yoke and the stator teeth; R_4 is the stator resistance and the stator winding thermal resistance; R_5 is the total air gap thermal resistance; R_6 is the permanent magnet thermal resistance; P_1 is the iron loss of the stator yoke; P_2 is the iron loss of the stator teeth; P_3 is the copper loss of the stator winding; P_4 is the wind friction loss; and P_5 is the eddy current loss of the permanent magnet.

The motor cooling design is based on the inlet temperature of 30 °C, with a cooling water flow rate of 1.25 m/s. The cross-section size and the number of spirals of the water channel are the main factors affecting the heat dissipation of the motor and the resistance of the water flow are primarily affected by the cross-section size and the number of spirals of the water channel. With this in mind, then, high heat dissipation and low water resistance can be taken as the two optimization goals of the cooling structure. In the temperature verification of the prototype, what needs to be initially determined is the thermal conductivity of the material. According to the cooling conditions and the speed, the thermal conductivity of each position of the prototype is shown in Table III. Temperature verification was performed in three operating states of the prototype base speed rated point, overload point and high speed point. The requirements for the temperature distribution of the motor are determined according to the insulation level of the motor material. Being that different insulation materials have differing capabilities in the withstanding of high temperatures, six allowable maximum temperatures are specified, arranged according to the temperature as Y, A, E, B, F and H, with respective permissible operating temperatures of 90, 105, 120, 130, 155 and 180 °C.

TABLE III
THERMAL CONDUCTIVITY OF DIFFERENT POSITIONS OF THE MOTOR

Components	Material	Thermal conductivity
iron core	steel sheet	40 W/m°C
winding	copper	360 W/m°C
magnet	NdFeB	8.8 W/m°C
gap	air	0.026 W/m°C

When the ambient temperature is 30 °C, the temperature distribution of three operating states of the motor are shown in Fig. 11 when the casing is water-cooled. It can be seen that the temperature of the motor increases along with the increase in current density and speed, where the effect of current density on the rise in temperature is more apparent. When the current density is 3.74 A/mm^2, the maximum temperature of the motor is 93.8 °C, which is located on the winding in the middle of the stator core. Each part of the motor can run at its own allowable temperature. The core and winding have a stable mechanical structure. The magnet does not undergo irreversible demagnetization and is thus able to keep the motor safe and stable for a long duration. When the current density is 8.57 A/mm^2, the maximum temperature of the motor is 177.3 °C. This design motor uses H-class insulation material, with a heat-resistant temperature of 180 °C that therefore meets the requirements.

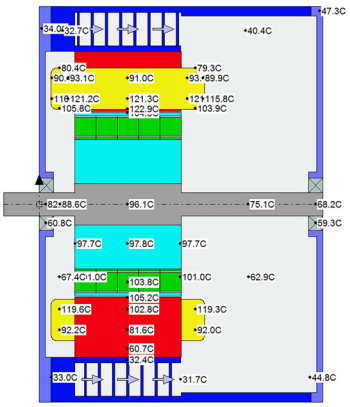

(a)

This article has been accepted for publication in a future issue of this journal, but has not been fully edited. Content may change prior to final publication. Citation information: DOI 10.1109/TTE.2020.2992901, IEEE Transactions on Transportation Electrification

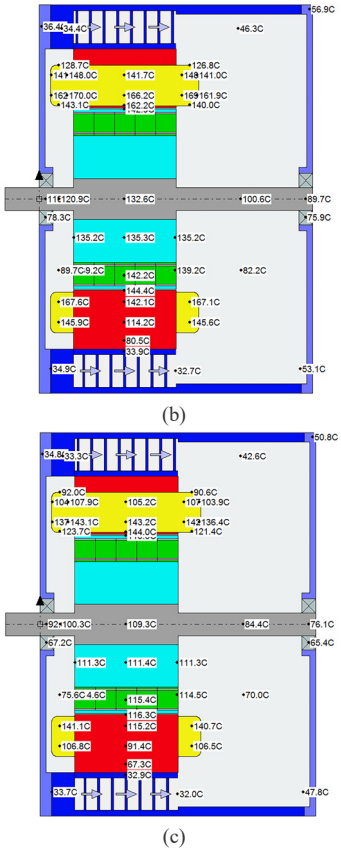

(b)

(c)

Fig. 11. Thermal distributions of IMMD at different operating conditions. (a) 3.74 A/mm^2 and 6, 000 rpm. (b) 8.57 A/mm^2 and 5, 000 rpm. (c) 4.91 A/mm^2 and 15, 000 rpm.

IV. Torque Ripple Suppression at High-speed Point

During the operation of the motor, the stability of the motor is affected by excessive torque ripple, leading to an increase in the loss of the motor. Torque ripple is predominantly divided into electromagnetic torque ripple and cogging torque, caused by harmonic and cogging effects, respectively. Therefore, torque ripple must be considered in the design process of the motor.

As the project uses fractional-slot windings, there are fewer cogging harmonics; however, fractional-slot windings do contain rich current harmonics. When the motor is running at a low speed, the internal power angle of the stator side current and the demagnetizing current component are both small, thereby having a small impact on the magnetic dense waveform in the air gap of the motor. Therefore, at the moment of overload and base speed, the torque ripple of the motor is relatively small at approximately 3%, but the internal power factor angle of the high-speed point is large. This generates a large demagnetizing magnetic field that results in a large distortion of the flux density waveform in the air gap of the motor, thereby causing a large distortion of the motor's terminal voltage waveform and a large output torque waveform. Therefore, the rotor structure needs to be optimized in order to reduce the air gap flux density distortion of the motor at high speed. To do this, it is necessary to perform segmented skewed pole processing on the rotor based on the original electromagnetic structure that is unchanged.

Rotor segmented skewed poles are usually able to reduce the tooth harmonics with a high degree of effectiveness. In addition, they are further able to achieve the effect of reducing the cogging torque and torque ripple of the motor. In theory, the rotor skewed pole can achieve the same effect as the skewed stator slot. Generally, the rotor has two methods: continuous and segmented skewed poles. A continuous skewed pole will produce the same result as the skewed stator slot, but will increase the production cost of the magnetic steel and so should generally not be used. The segmented inclined pole of the rotor can also achieve the purpose of weakening the cogging harmonics and reducing the cogging torque, where this inclined pole method does not lead to an increase in the production costs. The relationship between the segmented skewed pole of the rotor and the radial electromagnetic force is studied in-depth, with the equivalent skewed pole model being established using Maxwell. The three skewed pole modes are shown in Fig. 12.

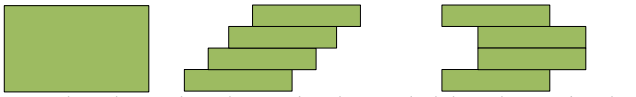

Fig. 12. Rotor segmented skewed pole method.

After the skewed pole method is selected, it is necessary to determine the skewed pole angle and the number of segments. After using Maxwell software is used to parameterize these two parameters, the following curves can be obtained.

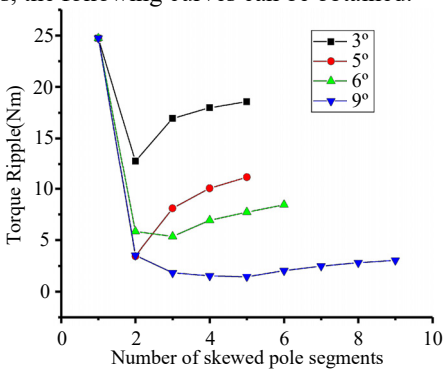

Fig. 13. Torque ripple of different skewed pole angles and number of segments in high-speed area.

As can be seen from Fig. 13, after the rotor segmented skewed poles are used, the torque ripple of the motor at a high-speed point can be significantly suppressed. The number of single rotor segments cannot be arbitrarily selected, with the number of rotor skewed pole segments being closely related to the angle of the rotor skewed poles. Before the rotor is not skewed, the peak torque of the output torque of the motor is 24.6 Nm and the torque ripple is 57.6%. As the number of skewed pole segments of the motor increases, the output torque ripple of the motor decreases before increasing. As can be seen from the above figures, when the skewed pole angle of the motor rotor is nine degrees and the number of skewed pole segments is three, the peak-to-peak torque is 1.46 Nm, the high-speed point output torque is 38.7 Nm, the torque ripple is 3.78%, and the torque ripple of the no skewed pole rotor is 57.6%. Therefore, the optimal skewed pole angle of the motor rotor is 9 degrees and divided into three segments. The single-shaped magnetic pole can significantly suppress the machine torque ripple in high speed areas.

This article has been accepted for publication in a future issue of this journal, but has not been fully edited. Content may change prior to final publication. Citation information: DOI 10.1109/TTE.2020.2992901, IEEE Transactions on Transportation Electrification

V. Conclusion

In this paper, key technologies of IMMD that are applied to aeronautical fields are proposed and researched. Taking into consideration the high requirements for driving motors in the aerospace field, this paper proposes a topology of integrating the motor and converter for a compact design. In order to improve the power density of the whole driving system, the influence of different slot-pole ratios on the performance of the motor are analyzed, where the structural layout of the fractional-slot distributed winding is determined. Unified cooling of the IMMD, where the motor and converter are cooled together, is adopted by the water-cooled housing so as to avoid the converter operating in a high temperature environment. By optimizing the analysis of the skew angles of the magnetic poles as well as the number of segments for the skewed rotor, the torque ripple of the IMMD is greatly reduced, enabling it to operate smoothly under different working conditions. In sum, the IMMD is able to effectively meet the requirements for the motors that are applied in more electric aircraft.

References

[1] F. J. Bartos, "Combination Motors and Drives Move to Make Their Mark," Control Engineering Online, December 2000, http://www.csemag.com/single-article/combination-motors-and-drives-move-tomake-their-mark/d9a8ab08897749f02e39653c06a6cc49.html

[2] X. Roboam, B. Sareni, and A. Andrade, "More Electricity in the Air: Toward Optimized Electrical Networks Embedded in More-Electrical Aircraft," *IEEE Ind Electron M.*, vol. 6, no. 4, pp. 6-17, Dec. 2012.

[3] P. N. Enjeti, W. Shireen, "A New Technique to Reject DC-link Voltage Ripple for Inverters Operating on Programmed PWM Waveforms," *IEEE Trans. Power Electron*., vol. 7, no. 1, pp. 171-180, Jan. 1992.

[4] W. P. Cao, B. C. Mecrow, G. J. Atkinson, J. W. Bennett, and D. J. Atkinson, "Overview of Electric Machine Technologies Used for More Electric Aircraft (MEA)," *IEEE Trans. Ind. Electron.*, vol. 59, no. 9, pp. 3523-3531, Sep. 2012.

[5] S. U. Chung, J. M. Kim, D. H. Koo, B. C. Woo, D. K. Hong, and J. Y. Lee, "Fractional Slot Concentrated Winding Permanent Magnet Synchronous Machine with Consequent Pole Rotor for Low Speed Direct Drive," *IEEE Trans. Magn*., vol. 48, no. 11, pp. 2965-2968, Dec. 2012.

[6] J. Wang, Y. Li, and Y. Han, "Integrated Modular Motor Drive Design with GaN Power FETs," *IEEE Trans. Ind. Appl.*, vol. 51, no. 4, pp. 3198-3207, Jan./Aug. 2015.

[7] M. D. Hennen, M. Niessen, C. Heyers, H. J. Brauer, and R. W. De Doncker, "Development and Control of an Integrated and Distributed Inverter for a Fault Tolerant Five-Phase Switched Reluctance Traction Drive," *IEEE Trans. Power Electron*., vol. 27, no. 2, pp. 547-554, Feb. 2012.

[8] Abebe, R., Vakil, G., Lo Calzo, G., Cox, T., Lambert, S., Johnson, M., Gerada, C., and Mecrow, B., "Integrated Motor Drives: State of the Art and Future Trends," *IET Elect. Power Appl*., vol. 10, no. 8, pp. 757-771, Sep. 2016.

[9] M. Villani, M. Tursini, G. Fabri, and L. Castellini, "High Reliability Permanent Magnet Brushless Machine Drive for Aircraft Application," *IEEE Trans. Ind. Electron*., vol. 59, no. 5, pp. 2073-2081, May 2012.

[10] A. M. EL-Refaie, M. R. Shah, R. H. Qu, and J. M. Kern, "Effect of Number of Phases on Losses in Conducting Sleeves of Surface PM Machine Rotors Equipped with Fractional-Slot Concentrated Windings," *IEEE Trans. Ind. Appl.*, vol. 44, no. 5, pp. 1522-1532, Sep./Oct. 2008.

Shaopeng Wu (S'10–M'11–SM'19) was born in Linkou, Heilongjiang, China, in 1983. He received the B.S., M.S., and Ph.D. degrees in electrical engineering from the Harbin Institute of Technology (HIT), Harbin, China, in 2005, 2008, and 2011, respectively.

He was a Visiting Scholar of Wisconsin Electric Machines and Power Electronics Consortium (WEMPEC) with the University of Wisconsin-Madison, Madison WI, USA, from 2013 to 2014. He is currently an Associate Professor with HIT. His current research interests include the design and control of special electric machines, the research of multi-physical coupling, and the related technologies in electromagnetic launch field.

Dr. Wu was a recipient of the Peter J. Kemmey Memorial Scholarship Award by the 15th International EML Symposium, Brussels, Belgium, in 2010.

Chenchen Tian was born in Henan, China, in 1996. He received the bachelor's degree from Harbin Institute of Technology (HIT) in 2018. He is currently studying for a master's degree in motors and electrical appliances. His research interests include machine design and temperature field design.

Weiduo Zhao was born in Harbin, China, in 1985. He received the bachelor's degree in electrical engineering from the Taiyuan University of Technology, Taiyuan, China, in 2008, and the M.Sc. degree and Ph.D. degree in electrical engineering from the Harbin Institute of Technology, Harbin, China, in 2010 and 2015, respectively.

He is currently a senior research fellow with the Power Electronics, Machines and Control Group, The University of Nottingham, Ningbo, China. His research interests include high-performance electric machines and drives, pulsed power systems, and thermal management.

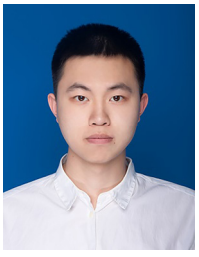

Jinyang Zhou was born in Shenyang, China, in 1998. He is currently an undergraduate at shenyang university of technology and will be admitted to Harbin Institute of Technology in 2020, where he will pursue a master's degree in electrical engineering. His research focuses on electrical machine design.